



**HAL**  
open science

## **3-Hydroxypyridinyl-Substituted-1,2,4-Triazoles as New ESIPT Based Fluorescent Dyes: Synthesis and Structure–Fluorescence Properties Correlations**

Anthony Nina-Diogo, Benoît Bertrand, Serge Thorimbert, Geoffrey Gontard,  
Sehr Nassem-Kahn, Andrea Echeverri, Julia Contreras-García, Clémence  
Allain, Gilles Lemercier, Eleonora Luppi, et al.

### ► To cite this version:

Anthony Nina-Diogo, Benoît Bertrand, Serge Thorimbert, Geoffrey Gontard, Sehr Nassem-Kahn, et al.. 3-Hydroxypyridinyl-Substituted-1,2,4-Triazoles as New ESIPT Based Fluorescent Dyes: Synthesis and Structure–Fluorescence Properties Correlations. *Advanced Optical Materials*, 2023, 11 (14), pp.2300336. 10.1002/adom.202300336 . hal-04076746

**HAL Id: hal-04076746**

**<https://hal.science/hal-04076746>**

Submitted on 21 Apr 2023

**HAL** is a multi-disciplinary open access archive for the deposit and dissemination of scientific research documents, whether they are published or not. The documents may come from teaching and research institutions in France or abroad, or from public or private research centers.

L'archive ouverte pluridisciplinaire **HAL**, est destinée au dépôt et à la diffusion de documents scientifiques de niveau recherche, publiés ou non, émanant des établissements d'enseignement et de recherche français ou étrangers, des laboratoires publics ou privés.

## Advancing Characterization of Materials by Multimodal 4D-STEM Analytical Methods

April 26, 11:00am - 12:00pm EDT

Development and production of new materials and semiconductor devices require morphological, structural, and chemical characterization at the nanoscale level to understand their chemico-physical properties and optimize their production process. Besides traditional electron microscopy imaging and compositional analysis techniques, 4D-STEM methods provide additional structural information about the local internal organization of atoms and molecules at each position of an acquired STEM map.

Watch this session during the WAS Virtual Conference:



Dr. Daniel Nemecek



Dr. Tingting Yang

[Register Now](#)

# 3-Hydroxypyridinyl-Substituted-1,2,4-Triazoles as New ESIPT Based Fluorescent Dyes: Synthesis and Structure–Fluorescence Properties Correlations

Anthony Nina-Diogo, Benoît Bertrand, Serge Thorimbert, Geoffrey Gontard, Sehr Nassem-Kahn, Andrea Echeverri, Julia Contreras-García, Clémence Allain, Gilles Lemerrier, Eleonora Luppi, and Candice Botuha\*

This report presents the design, synthesis, and photophysical study of two new series of promising fluorescent trisubstituted triazoles, 3-hydroxypyridinyl substituted-1,2,4-triazoles (PyOHTr) and 2-pyridonyl substituted-1,2,4-triazoles (PyCOTr). An excited state intramolecular proton transfer (ESIPT) fluorescence mechanism is evidenced for PyOHTr molecules by *ab initio* theoretical calculations. These fluorescent dyes possess unique optical properties such as large Stokes shifts, dual emission, solvatochromism, solid-state emission and, for one of them, a white light emission, rendering them particularly attractive for future applications in both medicinal chemistry and materials science.

## 1. Introduction

Fluorophores exhibiting phototautomerization via an excited state intramolecular proton transfer (ESIPT) are highly required in order to develop optoelectronic devices, such as organic light-emitting diode materials, fluorescent sensors for the detection of small molecules, proteins, cations, and UV stabilizers in polymers or sun cream.<sup>[1]</sup> ESIPT emission arises from a proton-transfer species generated by the photoexcitation of an intramolecular hydrogen-bonded molecule bearing a proton donor group, mostly a hydroxyl or a phenol group and a neighboring basic proton acceptor,

usually a heterocyclic nitrogen atom or a carbonyl oxygen atom. Due to the intramolecular hydrogen bonding site, ESIPT fluorophores are sensitive to the environment (i.e., pH, polarity of the solvent, presence of ions ...), which often lead to a dual emission: a normal fluorescence from enol tautomer E\* and an ESIPT fluorescence from keto tautomer K\* at longer wavelength with a large Stokes shift preventing the self-quenching fluorescence. In apolar solvents more particularly, or with metal complexation conditions reinforcing the formation of strong intramolecular hydrogen bond, ESIPT fluorophores may exhibit a panchromatic spectrum with several emitting species covering visible light range from blue to red with high quantum yields and bright luminescence even in solid state.<sup>[2a]</sup> It may lead to a white light emission and promising candidates as single component white light generators.<sup>[2]</sup>

In most cases, upon excitation, ESIPT fluorophores undergo keto-enol type tautomerization. To date only few types of ESIPT dyes of different structure have been reported due to the requirement of particular structural arrangements, planar system and hydrogen bonding ability. Among them one can mention 2-hydroxyphenyl benzothiazole (HBT), 2-(2'-hydroxyphenyl) benzoxazole (HBO) and flavones with a phenolic OH donating group acting as a proton donor which have been attracting great interest in several areas.<sup>[3]</sup> However ESIPT systems possessing other types of phenol OH donating groups are less studied, albeit very promising for the development of a new class of ESIPT fluorophores. Consequently, due to their unique optical properties, engineering of new class ESIPT fluorophores with large Stokes

A. Nina-Diogo, B. Bertrand, S. Thorimbert, G. Gontard, C. Botuha  
Institut Parisien de Chimie Moléculaire  
CNRS


Sorbonne Université  
Paris 75252, France  
E-mail: Candice.botuha@sorbonne-universite.fr

S. Nassem-Kahn, A. Echeverri, J. Contreras-García, E. Luppi  
Laboratoire de chimie théorique Paris  
CNRS

Sorbonne Université  
Paris 75252, France

C. Allain  
PPSM  
CNRS  
ENS Paris-Saclay  
Université Paris-Saclay  
Gif-sur-Yvette 91190, France

G. Lemerrier  
Institut de Chimie Moléculaire de Reims (ICMR)  
CNRS  
Université de Reims Champagne-Ardenne  
Moulin de la Housse, BP 1039, 51687 Reims Cedex 2, France

 The ORCID identification number(s) for the author(s) of this article can be found under <https://doi.org/10.1002/adom.202300336>

© 2023 The Authors. Advanced Optical Materials published by Wiley-VCH GmbH. This is an open access article under the terms of the Creative Commons Attribution License, which permits use, distribution and reproduction in any medium, provided the original work is properly cited.

DOI: 10.1002/adom.202300336

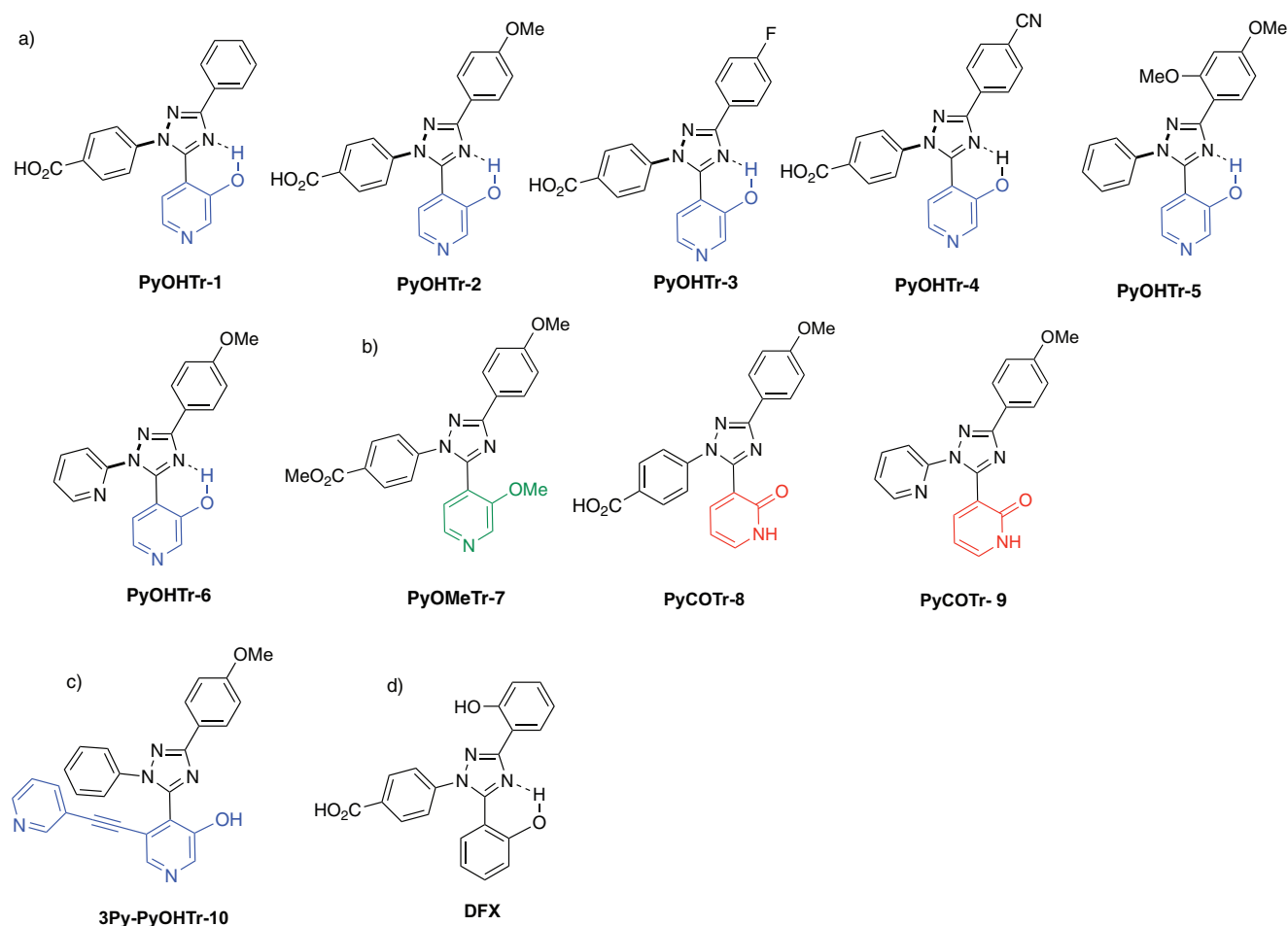


**Figure 1.** Molecular structures of fluorescent triazoles studied in this work. a) PyOHTr-1 from Series 1 with an intramolecular H bonding. b) PyOMeTr-7 with no H bonding and PyCOTr-8 and 9 from Series 2. c)  $\pi$ -extended 3Py-PyOHTr-10 and d) nonfluorescent Deferasirox (DFX).<sup>[4]</sup>

shift, high photostability and dual fluorescence continue to be an active and competitive area of research for both fundamental and application point of view.

We previously reported a rapid synthesis of hydroxypyridyl-1,2,4-oxadiazoles, -1,3,5-triazines and -1,2,4-triazoles,<sup>[5]</sup> and later synthesized two specimens of  $\pi$ -conjugated 2-hydroxypyridyl-1,2,4-triazoles with promising fluorescent properties.<sup>[6]</sup> An unexpected extremely large Stokes shift over 10 000  $\text{cm}^{-1}$  was observed in organic solvents which was suggested to be originated from an ESIPT between the hydroxyl group of the pyridol ring and the triazole moiety. These structures can be considered as luminescent pyridyl analogs of well-known 1,2,4-triazoles<sup>[7]</sup> such as Deferasirox (DFX), an iron chelator used in medicine, which possesses two phenolic units attached to a 1,2,4-triazoles core and which is not luminescent in both aqueous and organic solvents.<sup>[8]</sup>

Interestingly, some  $\pi$ -conjugated 1,3,5-trisubstituted-1,2,4-triazoles have already shown photoluminescence properties and have been used as selective sensors for metal cations.<sup>[9,10]</sup> In addition, tridentate complexes of DFX with platinum(II) bearing a bis-aryloxy 1,2,4-triazole ligand<sup>[11]</sup> or 1,2,4-triazoles with benzothiazole fragment<sup>[12]</sup> have shown promising photoluminescence properties to be further exploited in devices for opto-

electronic applications. A double ESIPT emission of 3,5-bis(2-hydroxyphenyl)-1H-1,2,4-triazoles has also been reported.<sup>[13]</sup> More recently, DFX derivatives bearing a phenyl and a benzothiazole moiety instead of the 4-benzoic acid fragment in the triazole core have shown interesting fluorescence properties in aqueous media arising from a combined ESIPT-aggregation induced emission affording a potential novel diagnostic platform for bacteria biofilm studies.<sup>[14]</sup> However, little is known about pyridyl substituted 1,2,4-triazoles<sup>[15]</sup> and nothing about hydroxypyridyl-triazoles.

In the present work and motivated by our previous studies on triazoles, we designed and synthesized two series of molecules which we report in **Figure 1**. Series 1 is composed by seven trisubstituted 3-hydroxypyridinyl-substituted-1,2,4-triazoles PyOHTr-1 to PyOHTr-6 and 3Py-PyOHTr-10, all possessing an intramolecular hydrogen bond while Series 2 is composed by two 2-pyridonyl-substituted-1,2,4-triazoles PyCOTr-8 and PyCOTr-9 isomers of Series 1 and the stand-alone full O-protected triazole PyOMeTr-7.

In order to confirm and explore the specific ESIPT phenomena for all the triazoles, we have thoroughly examined the effect on the fluorescence properties of the N atom position on the pyridol ring of Series 1 and 2 molecules. To modulate the electronic

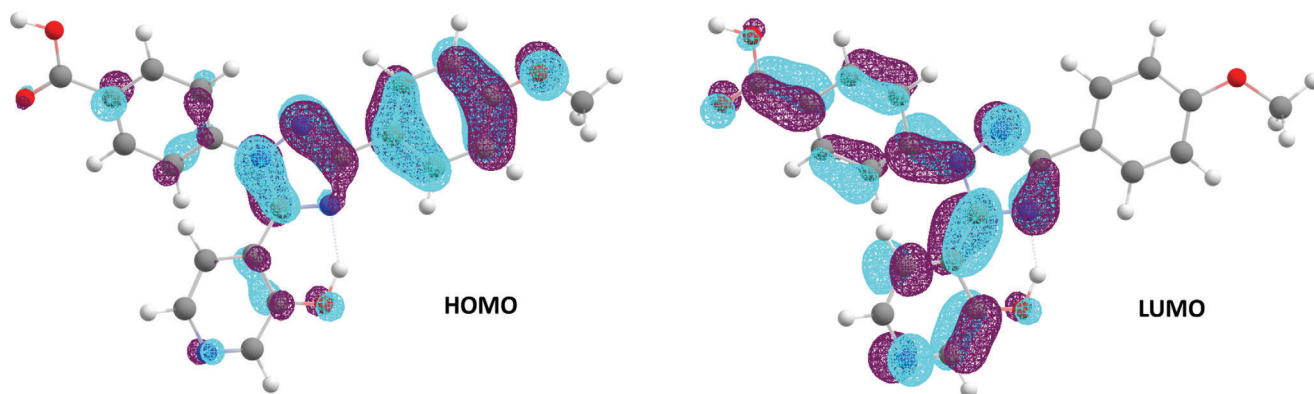


**Figure 2.** Ground-state HOMO (left) and LUMO (right) molecular orbitals for PyOHTr-2 in the enol open form.

nature of the system, we also extended the  $\pi$ -conjugation on the pyridol ring by adding an external 3-pyridinyl-alcynyl group in 3Py-PyOHTr-10. Moreover, the molecules of Series 2 and the PyOMeTr-7 have been designed with no intramolecular hydrogen bonding, which is supposed to inhibit the ESIPT process. Finally, ab initio theoretical calculations have been carried out for studying ground- and excited state properties in order to rationalize the experimental results.

## 2. Results and Discussion

The electronic properties and the molecular design of the triazoles of Figure 1 have been investigated with density functional theory (DFT) and time-dependent density functional theory (TD-DFT). The ground state geometry optimization of the molecular structures was performed with DFT using the B3LYP functional and the 6-31+G\* basis set. Instead, the calculation of the absorption  $S_0$ - $S_1$  and the corresponding emission was performed using TD-DFT with the CAM-B3LYP functional and still using the 6-31+G\* basis set. Moreover, all the calculations were performed with the polarized continuum model (PCM) in order to simulate the acetonitrile polar solvent.

Concerning Series 1, we report the theoretical calculations of PyOHTr-2 where the 3-hydroxy-1-pyridinyl-1,2,4-triazole is substituted by a 4-methoxyphenyl group at the C3 position and a 4-benzoic acid group at the N1 position of the triazole ring. We have chosen PyOHTr-2 because it is representative of the behavior of the PyOHTr-1 and PyOHTr-3-6 triazoles of Series 1.

In **Figure 2**, the optimized structure of PyOHTr-2 together with HOMO and LUMO molecular orbitals is shown. We observed that in the ground-state the PyOHTr-2 has an intermolecular hydrogen-bond, i.e., enol open form ( $E_{GS(open)}$ ). Moreover, studying and analyzing the  $S_0$ - $S_1$  transition (ground singlet state  $S_0$  to first excited state  $S_1$ ) we found that it is essentially due to a single excitation from the highest occupied molecular orbitals (HOMO) mainly localized on the phenyl ring to the lowest unoccupied molecular orbitals (LUMO), mainly involving the carboxylic acid function; they are spatially well separated on the molecule (Figure 2), which gives to this transition a charge-transfer character. This allowed us to design the substituents to decrease the HOMO–LUMO gap (see triazoles of Figure 1) and thus improving the absorption properties by shifting the absorption band

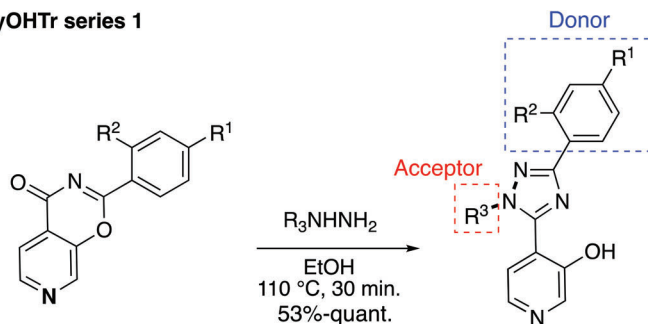
to higher wavelengths (red shift). In fact, whereas the HOMO is mainly located on the 4-methoxy phenyl substituent at the C3-position of the triazole ring, i.e., donor part (D), the LUMO is mainly located on the 4-benzoic acid substituent at the N1-position of the triazole ring, i.e., the acceptor part (A). This result suggests an intramolecular charge-transfer (ICT) process from the donor to the acceptor in the first excited state. Consequently, the C3-position of the triazole of PyOHTr series would be the optimal site for a substitution with an electron-rich arene (D) and the N1 position with an electron-withdrawing arene (A) in order to improve an ICT process (**Scheme 1**).

To complete the theoretical analysis of molecules of Series 1 we also calculated the photophysical properties of 3Py-PyOHTr-10 (Figures S36–S43, Supporting Information). Indeed, as this molecule has an extended  $\pi$ -conjugation with the pyridol ring, its optical behavior cannot be represented by PyOHTr-2. In the case of Series 2, for which no intramolecular H bonding was expected, we showed on the basis of theoretical calculations, that PyOHTr-8 can be taken as a representative molecular structure (see Figures S44–S46, Supporting Information).

Synthesis of functionalized 3-hydroxypyridinyl substituted-1,2,4-triazoles PyOHTr and 2-pyridonyl substituted-1,2,4-triazoles PyCOTr was achieved from the corresponding 4H-pyrido[4,3-e][1,3]oxazin-4-one PyOxa via an addition, ring opening, and ring closure (ANRORC) rearrangement (Figure 1).<sup>[4]</sup> The reaction was performed on pyridoxazinones PyOxa-1 to PyOxa-5 (Series 1) and PyOxa-6 (Series 2) using 4-hydrazino benzoic acid, phenyl- and 2-pyridyl hydrazine ( $R^3 = 4\text{-CO}_2\text{H-Ph}$ , Ph, 2-pyr) as nucleophiles in ethanol (EtOH) at 110 °C for 30 min. Surprisingly, the conversion of PyOxa-6 into triazole was ineffective in ethanol under standard heating conditions. Addition of 40% of acetic acid (AcOH) and heating in EtOH at 110 °C for 40 min helped the dehydration step to proceed and to get ring closure (**Scheme 1**, Series 2). Starting from 4-substituted phenyl rings ( $R^1$  and  $R^2$ ) with electron donating or -withdrawing groups, the corresponding 1,2,4-triazoles were obtained in good yield. The full O-protected triazole PyOMeTr-7, which may induce ESIPT process inhibition was synthesized from the corresponding pyridol PyOHTr-2 by addition of two equivalents of sodium hydride (NaH) and methyl iodide (MeI) (**Scheme 1**).

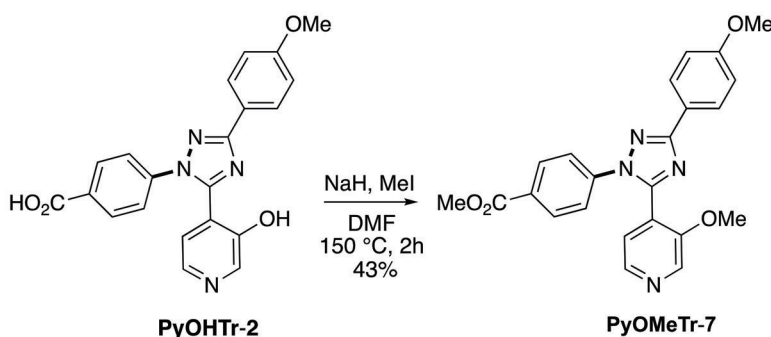
Single crystals of two representative tautomers of hydroxyl pyridyl triazoles (PyOHTr-5 and PyCOTr-9) suitable for X-ray

PyOHTr series 1

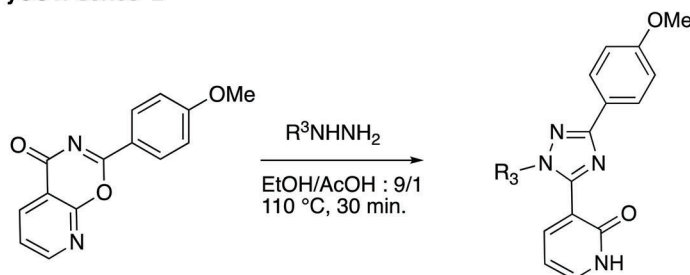


PyOXa-1 ( $R^1, R^2 = H$ )  
 PyOXa-2 ( $R^1 = OMe, R^2 = H$ )  
 PyOXa-3 ( $R^1 = F, R^2 = H$ )  
 PyOXa-4 ( $R^1 = CN, R^2 = H$ )  
 PyOXa-5 ( $R^1 = OMe, R^2 = OMe$ )

PyOHTr-1 ( $R^1, R^2 = H; R^3 = 4-CO_2H-Ph$ ), 53%  
 PyOHTr-2 ( $R^1 = OMe, R^2 = H; R^3 = 4-CO_2H-Ph$ ), quant.  
 PyOHTr-3 ( $R^1 = F, R^2 = H; R^3 = 4-CO_2H-Ph$ ), 78%  
 PyOHTr-4 ( $R^1 = CN, R^2 = H; R^3 = 4-CO_2H-Ph$ ), 66%  
 PyOHTr-5 ( $R^1, R^2 = OMe, R^3 = Ph$ ), 72%  
 PyOHTr-6 ( $R^1 = OMe, R^2 = H; R^3 = 2-Pyr$ ), 74%



PyCOTr series 2



PyOXa-6

PyCOTr-8 ( $R^3 = 4-CO_2H-Ph$ ), quant.  
 PyCOTr-9 ( $R^3 = 2-Pyr$ ), 77%

Scheme 1. Synthesis of PyOHTr and PyCOTr triazoles (Series 1 and 2).

analysis were obtained by slow evaporation of a concentrated solution in dichloromethane. The crystal structure of PyOHTr-5 shows a very strong intramolecular hydrogen bond between the hydroxyl group and a nitrogen N4 of the triazole ring. This is evidenced by the O1...N4 distance (2.585(2) Å) and the dihedral angle (1.04(22)°) between the pyridol ring and the triazole core, which maintain the triazole-pyridol system in a planar conformation (Figure 3, view B). Molecules are arranged in stacks with weak  $\pi$ - $\pi$  interactions (shortest distances 3.5–3.7 Å) (Figure 3, view C). On the other hand, PyCOTr-9 shows

no intramolecular interaction, as expected for 2-pyridone structures which are predominant in the crystalline state.<sup>[16]</sup> Instead, a dimer is formed via two intermolecular weaker hydrogen bonds (O1...N1 2.750(2) Å) in between two pyridines (see Figure S1, Supporting Information).<sup>[17]</sup>

Conformational studies of both series of triazoles in solution have been investigated. Previously, it is noteworthy to mention that due to their high lipophilicity (Log  $P = 6.3$  at pH 7.4 for DFX),<sup>[18]</sup> and their ability to be involved in  $\pi$ -stacking, all the triazoles described in this article including DFX are insoluble in

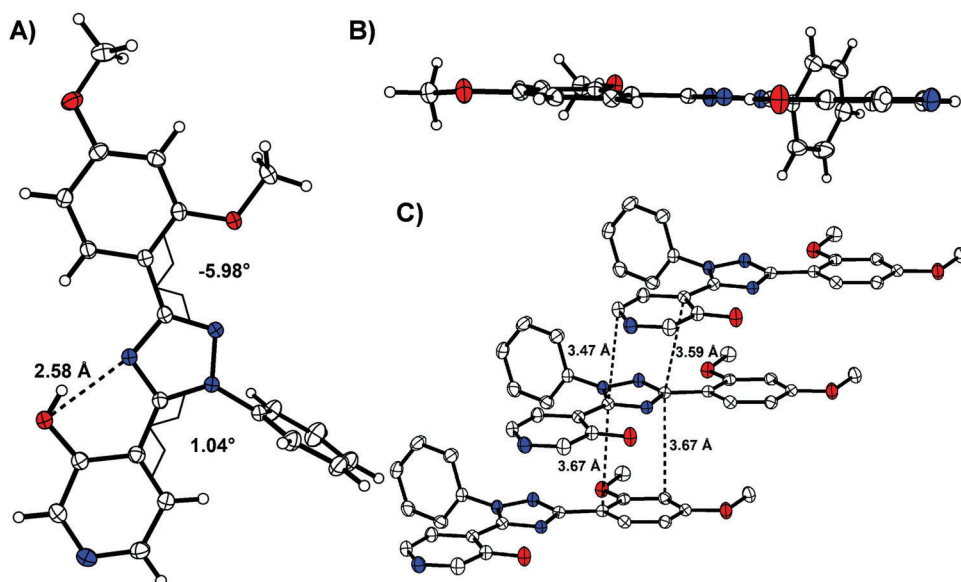


**Figure 3.** X-ray diffraction structure of PyOHTr-5. A) Front view, B) side view, and C) interactions and distances between stacks. Hydrogens omitted for clarity in (C) and thermal ellipsoids at 30% probability.

most of the solvents except in dimethylsulfoxide (DMSO). Consequently, the photophysical analyses have been performed by presolubilizing the compounds in DMSO at  $10^{-3}$  M and used it as mother solution to prepare  $10^{-5}$  M diluted solutions in various solvents. In the  $^1\text{H}$  NMR spectra in  $\text{DMSO-d}_6$ , the aromatic protons of PyOHTr-1 to PyOHTr-3 were observed between 7.0–8.3 ppm whereas the labile protons of pyridol group (C3-OH) and of carboxylic group (C4'-CO<sub>2</sub>H) were detected as broad singlets at 10.5 and 13.2 ppm, respectively (Figure S2, Supporting Information). Generally,  $\text{DMSO-d}_6$  reduces proton exchange rate and thus OH signal line widths due to its solvation ability.<sup>[19]</sup> In the case of PyOHTr compounds, the observed broad resonances were compatible with an intermolecular hydrogen bonding with residual  $\text{H}_2\text{O}$  or  $\text{DMSO-d}_6$ . In addition, the chemical shift of OH in the pyridol was not deshielded as it has been observed for strong intramolecular H-bonded OH in phenol such DFX. The mentioned spectra features are in accordance with an open enol form hydrogen-bonded to the polar solvent at the ground state. As for PyCOTr-8 from Series 2, the  $^1\text{H}$ -NMR spectroscopy studies in polar solvents like  $\text{DMSO-d}_6$  show the presence of typical chemical shifts of 2-pyridone structure: N1-H at 12.0 ppm and C5-H shielded at 6.4 ppm.<sup>[20]</sup> These observations confirm that 2-pyridone structure is the predominant tautomer of PyCOTr-8 in solution and thus evidences the absence of any intramolecular H-bond in  $\text{DMSO-d}_6$  (Figure S2, Supporting Information).

We have next studied the photophysical properties of all the triazoles dyes in different solvents and in solid state and reported the results in Table 1 (the spectra are available in the Supporting Information). Figure 4 displays the normalized absorption spectra of PyOHTr-2 in various solvents. Importantly, the absorption behavior of PyOHTr-2 is representative of the absorption behavior of other molecules belonging to Series 1, except 3Py-PyOHTr-10.

The maximum absorption of PyOHTr-2 assigned to a  $\pi$ - $\pi^*$  transition,<sup>[21]</sup> appears around 265 nm in all solvents with a high

molar absorption coefficient ( $38\,900\ \text{M}^{-1}\text{cm}^{-1}$  in  $\text{CH}_3\text{CN}$ ). This band shows a weak dependency to the polarity of the solvent suggesting the presence of the same conformer of PyOHTr-2 in the ground state, i.e., the open enol form  $E_{\text{GS}(\text{open})}$  hydrogen-bonded to the solvent (see Figure 7).<sup>[12]</sup> A less-intense long-wavelength band around 310 nm is also observed mainly in  $\text{CH}_3\text{CN}$  and  $\text{CH}_2\text{Cl}_2$ . Interestingly, this less intense long-wavelength band slowly vanishes in a protic solvent (EtOH) and another long wavelength band at 350 nm appeared in  $\text{H}_2\text{O}$ .

As a general trend, similar absorption spectra were observed for all PyOHTr triazoles from Series 1 whatever the electronic substitution on the phenyl ring (Table 1 and spectra in the ESI). Absorption maxima were observed from 252 to 281 nm ( $\epsilon = 19\,600$  to  $37\,700\ \text{M}^{-1}\text{cm}^{-1}$  in  $\text{CH}_3\text{CN}$ ) with a weaker band at around 310–320 nm ( $\epsilon = 5\,500$  to  $6\,300\ \text{M}^{-1}\text{cm}^{-1}$  in  $\text{CH}_3\text{CN}$ ) in nonaqueous solvents. An additional band at 293 nm was observed for PyOHTr-5 possessing a 2,4-OMe-phenyl group Figure S15 (Supporting Information). Profile of absorption spectra recorded in all solvents for PyCOTr-8 from Series 2 were slightly different from those obtained for PyOHTr-2 showing vibrational bands in 260–340 nm area albeit with a similar maximum absorption around 260 nm ( $\epsilon = 23\,100\ \text{M}^{-1}\text{cm}^{-1}$ ) in  $\text{CH}_3\text{CN}$  (Figure S24, Supporting Information).

The emission spectra of triazoles were recorded in polar ( $\text{CH}_3\text{CN}$ , EtOH, and  $\text{H}_2\text{O}$ ), less polar ( $\text{CH}_2\text{Cl}_2$ ) solvents, and also in solid state (Table 1). In contrast with absorption spectra, fluorescence spectra were solvent and substitution dependent on triazole's series. As reported by Sessler et al.<sup>[13]</sup> we also confirmed the nonluminescent character of DFX.

First, solvent effect on fluorescence spectra was investigated. Emission spectra of the representative PyOHTr-2 from Series 1 were recorded as shown in Figure 5. Upon excitation at 270 nm in polar solvent  $\text{CH}_3\text{CN}$ , a broad spectrum with emission maximum at 419 nm and a shoulder band at around 480 nm were observed. In addition, a large Stokes shift of  $14\,200\ \text{cm}^{-1}$  for the

**Table 1.** UV–Vis absorption and fluorescence emission properties of Compounds **1** to **10** in various solvents: dichloromethane (CH<sub>2</sub>Cl<sub>2</sub>), acetonitrile (CH<sub>3</sub>CN), ethanol (EtOH) and water (H<sub>2</sub>O).

Compounds	Solvent <sup>a)</sup>	UV–Vis <sup>b)</sup>	Fluorescence <sup>c)</sup>		
		$\lambda_{\text{abs}}$ [nm] ( $\epsilon$ )	$\lambda_{\text{em}}^{\text{E*}}$ [nm] / Stokes <sup>d)</sup> shifts [cm <sup>-1</sup> ]	$\lambda_{\text{em}}^{\text{E*}}$ [nm] / Stokes <sup>d)</sup> shifts [cm <sup>-1</sup> ]	$\Phi_{\text{F}}[\%]$ <sup>e)</sup>
PyOHTr-1	CH <sub>3</sub> CN	252 (20.8), 310 (6.4)	372/12800	486/19100	0.03
	CH <sub>2</sub> Cl <sub>2</sub>	252, 320	371/12700	525/20600	
	EtOH	282	393/10000	486/14900	
	H <sub>2</sub> O	252, 350	434/16600	–	
PyOHTr-2	CH <sub>3</sub> CN	263 (37.7), 311 (10.3)	419/14200	483/17300	0.02
	CH <sub>2</sub> Cl <sub>2</sub>	263, 324	405/13300	514/18600	
	EtOH	261	417/14300	–	
	H <sub>2</sub> O	263, 340	–	–	
PyOHTr-3	CH <sub>3</sub> CN	255 (22.2), 316 (6.3)	379/12800	506/19500	0.02
	CH <sub>2</sub> Cl <sub>2</sub>	255, 324	379/12800	516/19800	
	EtOH	273, 290	386/10700	–	
	H <sub>2</sub> O	255, 348	428/15900	–	
PyOHTr-4	CH <sub>3</sub> CN	277, 318	375/9400	–	0.01
	CH <sub>2</sub> Cl <sub>2</sub>	279, 316	372/9000	521/16600	
	EtOH	281	376/9000	427/12200	
	H <sub>2</sub> O	271, 348	432/13800	–	
PyOHTr-5	Solid	–	–	501/9000 <sup>f)</sup>	< 0.01
	CH <sub>3</sub> CN	257 (19.6), 296 (12.0), 321 (7.0)	416/14900	494/18700	
	CH <sub>2</sub> Cl <sub>2</sub>	257, 293, 321	–	497/18800	
	EtOH	257, 290, 329	407/14300	488/18400	
	H <sub>2</sub> O	255, 296, 333	–	–	
PyOHTr-6	Solid	–	–	471/7800 <sup>f)</sup>	0.10
	CH <sub>3</sub> CN	265 (29.1), 324 (5.5)	415/13600	470/16500	
	CH <sub>2</sub> Cl <sub>2</sub>	266, 324	408/13100	518/18300	
	EtOH	266	427/14200	446/15200	
	H <sub>2</sub> O	263, 350	–	–	
PyOMe-Tr-7	Solid	–	–	491/8200 <sup>g)</sup>	0.14
	CH <sub>3</sub> CN	260 (26.1)	423/14800	–	
	CH <sub>2</sub> Cl <sub>2</sub>	263	410/13600	–	
	EtOH	259	426/15100	–	
PyCOTr-8	H <sub>2</sub> O	259, 352	–	–	0.10
	CH <sub>3</sub> CN	261 (23.1), 283 (18.5), 302 (17.8),	409/13900	–	
	CH <sub>2</sub> Cl <sub>2</sub>	333 (8.0)	406/13400	–	
	EtOH	263, 287, 303, 338	406/13400	–	
PyCOTr-9	H <sub>2</sub> O	263, 284, 302 331	–	–	0.34
	Solid	264, 274, 323	–	–	
	CH <sub>3</sub> CN	261 (22.3), 282 (20.3), 301 (14.4),	406/13700	–	
	CH <sub>2</sub> Cl <sub>2</sub>	333 (9.8)	406/13700	–	
	EtOH	261, 284, 301, 331	406/13700	–	
3Py-PyOHTr-10	H <sub>2</sub> O	261, 282, 300, 329	–	–	0.20
	Solid	258, 331	–	–	
	CH <sub>3</sub> CN	266 (32.5), 329 (10.2)	–	507/17900	
	CH <sub>2</sub> Cl <sub>2</sub>	269, 326	413/13000	520/17900	
3Py-PyOHTr-10	EtOH	266, 338	430/14300	507/17900	0.20
	H <sub>2</sub> O	261, 343	–	–	

(Continued)



**Table 1.** (Continued).

Compounds	Solvent <sup>a)</sup>	UV-Vis <sup>b)</sup>		Fluorescence <sup>c)</sup>	
		$\lambda_{\text{abs}}$ [nm] ( $\epsilon$ )	$\lambda_{\text{em}}^{\text{Ex}}$ [nm] / Stokes <sup>d)</sup> shifts [ $\text{cm}^{-1}$ ]	$\lambda_{\text{em}}^{\text{Em}}$ [nm] / Stokes <sup>d)</sup> shifts [ $\text{cm}^{-1}$ ]	$\Phi_{\text{F}}[\%]$ <sup>e)</sup>
DFX	CH <sub>3</sub> CN	308 (10.8)	–	–	–
	CH <sub>2</sub> Cl <sub>2</sub>	301	–	–	–
	EtOH	294, 425	–	–	–
	H <sub>2</sub> O	284 <sup>h)</sup>	–	–	–

<sup>a)</sup> All compounds were presolubilized in DMSO at  $10^{-3}$  M and used it as mother solution to prepare  $10^{-5}$  M diluted solutions in solvents; <sup>b)</sup> Absorption maxima measured in solution ( $10^{-5}$  M) at room temperature in nm; extinction coefficient at absorption maxima in  $10^3 \text{ M}^{-1} \text{ cm}^{-1}$ ; <sup>c)</sup> Fluorescence wavelengths at room temperature at a concentration of  $10^{-5}$  M; <sup>d)</sup> Stokes shift in  $\text{cm}^{-1}$  defined as the wavelength difference between the absorption and emission peak maxima; <sup>e)</sup> Fluorescence quantum yields measured using a 0.1 M H<sub>2</sub>SO<sub>4</sub> solution of quinine sulfate ( $\varphi_{\text{F}} = 0.55$ ) as a reference. [22]; <sup>f)</sup> Excitation at 345 nm; <sup>g)</sup> Excitation at 350 nm; <sup>h)</sup> Literature: DFX : UV max DFX (H<sub>2</sub>O/DMSO, pH <2) : 284 nm ( $15 \times 10^3 \text{ M}^{-1} \text{ cm}^{-1}$ ).

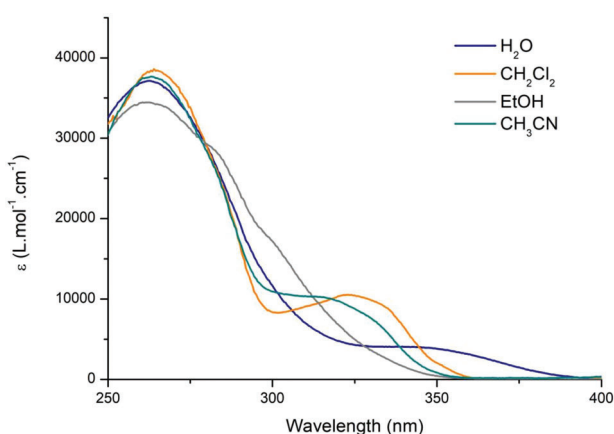


**Figure 4.** UV-Vis absorption spectra in various solvents for PyOHTr-2.

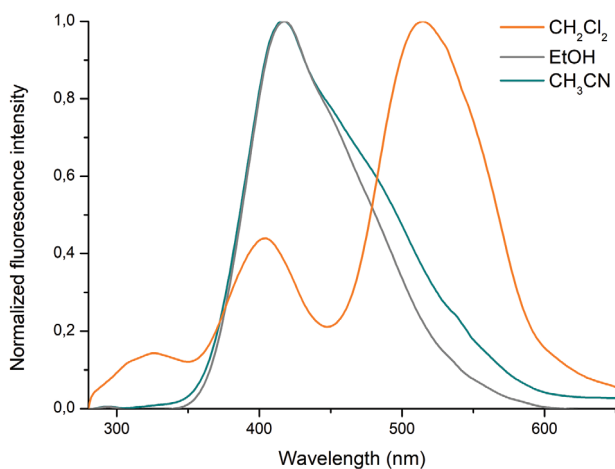


**Figure 5.** Normalized emission spectra of PyOHTr-2 ( $10 \times 10^{-6}$  M) recorded in different solvents.  $\lambda_{\text{exc}} = 270$  nm.

first emission and a low quantum yield ( $\varphi_{\text{F}} = 0.02$ ) were also observed (Figure 5 and Table 1). This low emission quantum yield was attributed to a nonradiative loss of energy, which is common for deactivation pathway during charge transfer. A similar maximum emission at 417 nm was obtained in EtOH, whereas in H<sub>2</sub>O, the fluorescence was totally quenched.

The time-resolved fluorescence decays were also recorded at different emission wavelengths in acetonitrile (400, 435, and 500 nm, see Figure S8, Supporting Information). Decays were fitted using four-time constants (see Table S1, Supporting Information) using a global analysis. These complex decays in solution attest for the existence of several emissive states, which is fully compatible with the dual emission from enol E\* (419 nm) and keto K\* (483 nm) conformers.

Excitation spectra recorded at the two different emission wavelengths (421 and 482 nm) are identical (see spectra in Figure S6, Supporting Information). This is in agreement with the presence of only one conformer at the ground state which we believe to be the most stable open enol form E<sub>GS(open)</sub>.

Interestingly, in less polar solvent CH<sub>2</sub>Cl<sub>2</sub>, the irradiation of PyOHTr-2 solution produced weak dual emission with a low intensity band at 405 nm and a higher intensity band which predominate at 513 nm compatible with an ESIPT emission (Keto emission K\*).

Dual emission coming from ESIPT process is generally favored in a less polar solvent such as CH<sub>2</sub>Cl<sub>2</sub> privileging intramolecular hydrogen bonding and the enhancement of K\* emission.<sup>[1a]</sup> In CH<sub>2</sub>Cl<sub>2</sub>, the excitation spectra recorded for PyOHTr-2 at the shorter (405 nm) and the longer emission wavelength (513 nm) are not identical (see Figure S7, Supporting Information). This suggests the presence of different conformers in equilibrium besides the presence of the open-enol form E<sub>GS(open)</sub>. One conformer has a closed-enol form possessing an intramolecular H-bond. In CH<sub>2</sub>Cl<sub>2</sub>, this closed form is more favored due to the lack of intermolecular H-bond and can explain the presence of higher concentrations of the corresponding enol-closed form in the excited state. The presence of the keto form is still evident around 330 nm in the excitation spectrum (emission around 513 nm, see Figure S7, Supporting Information). The time-resolved emission decays recorded in CH<sub>2</sub>Cl<sub>2</sub> at 400 and 535 nm emission (see Figures S9 and Table S2, Supporting Information) can be respectively fitted with four and three decay times, including one decay time of 0.32 ns that is also observed in acetonitrile and thus could be tentatively attributed to enol emission, less sensitive to solvent polarity. Altogether these data suggest that the open-enol form is the ground state precursor for the high energy emission (405 nm) and the closed-enol form, the one for low energy emission (513 nm) resulting from the ESIPT process.

In order to provide evidences of the presence of ESIPT in PyOHTr-2, emission spectra were recorded for PyOMeTr-7, analogue of PyOHTr-2 in which ESIPT is excluded due to methyl ether group. A unique emission band located at 410–420 nm was observed in CH<sub>3</sub>CN, DCM, and EtOH as solvents (Figure S22, Supporting Information). Emission wavelengths and Stokes shift of PyOMeTr-7 were almost identical to that of PyOHTr-2 for the enol band, which indicates a similar geometry (open enol form) for these two compounds in the excited state. In addition, fluorescence quantum yield of PyOMeTr-7 increases to 0.14 in CH<sub>3</sub>CN; this is in accordance with a loss of nonradiative deactivation process with the absence of any proton transfer at the excited state.

We have next investigated fluorescence properties of triazoles PyCOTr-8 from Series 2 for which no ESIPT should occur due to the absence of an intramolecular hydrogen bonding. Emission spectra of PyCOTr-8 exhibited only one emission peak around 406 nm in various solvent upon excitation at 263 nm, very close to the high-energy emission of PyOHTr-2. Absence of any solvatochromism confirms the absence of ESIPT for PyCOTr-8. (Figure S25, Supporting Information). Quantum yield of PyCOTr-8 is higher than PyOHTr-2 in acetonitrile ( $\varphi_F = 0.10$  versus 0.02 for 2) demonstrating that without ESIPT nonradiative deactivation process arising from conformational change is limited. PyCOTr-8 exhibits an average fluorescence lifetime at 405 nm similar to that of PyOHTr-2 for the normal emission (1.06 ns) (Figure S27 and Table S3, Supporting Information).

Next, the fluorescence–structure relationship was analyzed by comparing the emission spectra of the triazoles from Series 1 and PyOMeTr-7 (Table 1), which possess different aryl substituent at the C3- position of the triazole (R<sup>1</sup>) where the HOMO electron density is mainly located. The results show that electronic variation at the 4-position of the phenyl ring has a significant impact on the emission maxima of E\* in CH<sub>3</sub>CN. As for PyOHTr-2, 5-6 and PyOMeTr-7, the presence of electron donating groups (4-MeO-Ph) attached to electron deficient triazole leads to a red-shifted emission of E\* revealing a donor–acceptor type system with improved ICT character.

Interestingly, in a less polar solvent (CH<sub>2</sub>Cl<sub>2</sub>), triazole PyOHTr-5 (2,4-OMe-Ph) exhibits ESIPT fluorescence as unique emission at 497 nm with very large stokes shift (18 800 cm<sup>-1</sup>). The increasing basicity of the triazole nitrogen involved in the H-bonded with the pyridol favors the intramolecular proton transfer and fast ESIPT process at the excited state. In addition, a little blue shift is observed for ESIPT emission when increasing electron density at the C3 position from 521 nm (PyOHTr-4) to 497 nm (PyOHTr-5) in CH<sub>2</sub>Cl<sub>2</sub>.

Modification of the electron density at the N1 for PyOHTr-2 (LUMO) by replacing the 4-CO<sub>2</sub>H-Ph group by 3-pyridyl group (PyOHTr-6) has no significant impact on the normal E\* and ESIPT emission K\* however an increase of the quantum yield to 0.1 is observed.

As for non-ESIPT PyCOTr-8 and PyCOTr-9 from Series 2, emission wavelengths were perfectly identical in all solvents (406 nm). Quantum yield fluorescence of PyCOTr-9 raised dramatically to 0.34 in CH<sub>3</sub>CN which is in good agreement with the absence of any proton transfer.

Importantly, triazoles PyOHTr-1 (Ph), PyOHTr-3 (4-F-Ph), and PyOHTr-4 (4-CN-Ph) containing substituent with electro-

withdrawing properties are emissive in aqueous media (430 nm) albeit with low quantum yield (<0.01) (Table 1, Figure 6 and Figures S4 and S11, Supporting Information).

Under irradiation at 365 nm, the crystalline powders of PyOHTr-4 and PyOHTr-6 were found to be strongly emissive by naked-eye with a light green color with a wavelength maximum at 501 and 491 nm, respectively. These two fluorescence maxima are near the ESIPT luminescence in apolar CH<sub>2</sub>Cl<sub>2</sub> with an apparent increase of intensity indicating that the emission of PyOHTr-4 and PyOHTr-6 in crystals might come from ESIPT species K\* as it has been observed for PyOHTr-2 (Figure 6).

In order to corroborate the experimental results, we first calculated theoretical absorption, emission, and ESIPT of PyOHTr-2. The same theoretical studies have been performed for 3Py-PyOHTr-10 and PyOHTr-8 shown in Figures S46 and S53 (Supporting Information). We performed DFT calculations of ground state structures of possible conformers and tautomers of PyOHTr-2 in polar aprotic solvent such as acetonitrile. We estimated the relative stability between the different conformers and we found a PyOHTr-2 structure with an intramolecular hydrogen-bond, i.e., enol-closed form, which is in average less stable of 12.4 kcal mol<sup>-1</sup> with E<sub>GS(open)</sub> (PyOHTr-2 with an intermolecular hydrogen bond). The potential keto form, resulting from the hydrogen transfer from pyridol to triazole nitrogen, was also investigated. In this case, less stable structures than E<sub>GS(open)</sub> of about 16.8 kcal mol<sup>-1</sup> were found (Figure 7).

The most stable solvated (CH<sub>3</sub>CN) open-enol form E<sub>GS(open)</sub> for PyOHTr-2 is reported in the diagram of Figure 7, together with the vertical excitations toward the corresponding Franck–Condon excited state E\*<sub>FC(open)</sub>. From this transition, one can obtain the theoretical absorption (S<sub>0</sub>-S<sub>1</sub>). We found a good agreement of the main absorption peak 275 nm (4.51 eV) with the experimental data 311 nm (3.99 eV).

Upon excitation, we studied the relaxation in the excited state of E\*<sub>FC(open)</sub>. Two relevant structures were found in different minima in the excited state surface: E\* and K\*. The E\* has still an enol form but closed, while K\* has a keto form. The calculated emission from E\* is 387 nm (3.21 eV) which suggests that the shorter-wavelength recorded at 419 nm (2.96 eV) in CH<sub>3</sub>CN is the normal-ICT emission: E<sub>GS(open)</sub> is excited to E\*<sub>FC(open)</sub> which relax to E\* which then emits. Instead, the calculated emission from K\* is 462 nm (2.68 eV) which confirms that the longest emission wavelength identified as a shoulder band around 483 nm (2.57 eV) is the ESIPT fluorescence: E<sub>GS(open)</sub> is excited to E\*<sub>FC(open)</sub> which undergoes an intramolecular proton transfer, therefore relaxing to K\* which then emits.

The calculations of absorption and emission for PyCOTr-8 are also in good agreement with experiments. In this case we do not expect ESIPT. We found that the calculated excitation from the ground state keto form K to the Franck–Condon K\*<sub>(FC)</sub> is 295 nm (4.20 eV) compared well to the experiment 261 nm (4.75 eV). Then, also for this molecule we relaxed K\*<sub>(FC)</sub> in the excited state and we found the keto form K\* which emits at 410 nm (3.02 eV). The emission from experiment has been measured at 409 nm (3.03 eV) (Figure S46, Supporting Information).

In summary, in-depth analysis of photophysical properties of two representative molecules, with and without potential ESIPT, has been carried out. Theoretical calculations and time-resolved fluorescence studies enabled us to clearly explain the ESIPT

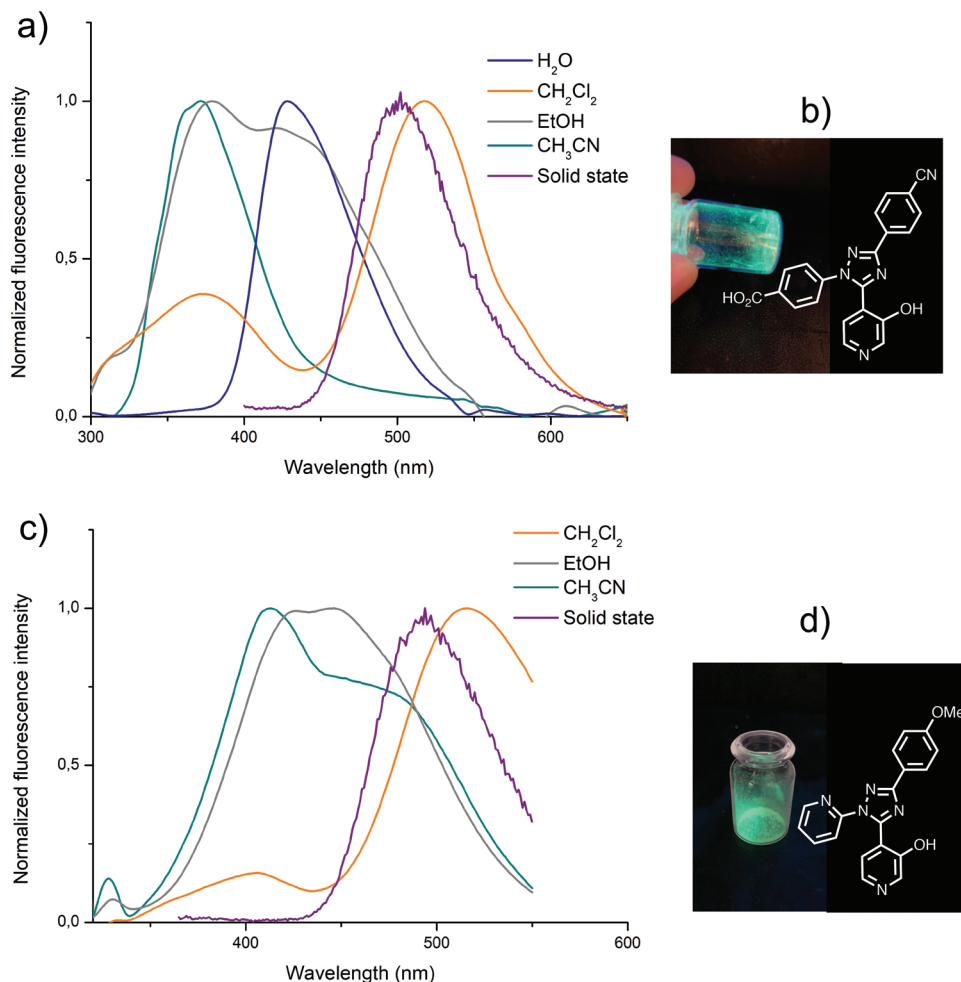


**Figure 6.** a) Emission spectra of PyOHTr-4 ( $\lambda_{\text{Exc}} = 270$  nm). b) Photographs of PyOHTr-4 under UV illumination at 365 nm in solid-state. c) PyOHTr-6 ( $\lambda_{\text{Exc}} = 300$  nm). The 2<sup>nd</sup> harmonic of the excitation wavelength has been removed for clarity. d) Photographs of PyOHTr-6 under UV illumination at 365 nm in solid state.

mechanism and give some insight of the structure–fluorescence relationship of these compounds.

At this stage, in order to modulate the electronic nature of the system, we have extended the  $\pi$ -conjugation on the pyridol ring by adding an external 3-pyridinyl-alkynyl group in 3Py-PyOHTr-10. We next studied the influence of  $\pi$ -expansion and conformational restriction of the PyOHTr core on the optical properties and measured emission characteristics. We hypothesized that expanded  $\pi$ -system will modify the energy levels and ICT characteristics of the newly obtained ESIPT compound and furnish bathochromic shifts in emission.<sup>[23]</sup>

Absorption wavelength maxima of the 3-pyridyl ethynyl substituted triazole, 3Py-PyOHTr-10<sup>[5]</sup> were observed in all solvent at 265 nm with a shoulder band around 320 nm, which is almost similar to the one obtained for its analogue PyOHTr-5. The presence of the  $\pi$ -extended conjugation on 3Py-PyOHTr-10 significantly affects fluorescence efficiency and emission characteristics. In aqueous media, 3Py-PyOHTr-10 is nonemissive while emissive in all tested organic solvents. Emission spectra exhibit large and intense green emission around 507–520 nm with a large Stokes shift up to 17 900  $\text{cm}^{-1}$  in CH<sub>2</sub>Cl<sub>2</sub> likely the keto

emission  $\text{K}^*$  associated to a weak shorter emission of the enol emission at 413 nm (Figure 8 and Figure S34, Supporting Information, for the International Commission of Illumination (CIE) coordinate. Interestingly, a significant higher quantum yield ( $\varphi_{\text{F}} = 0.20$ ) is obtained in acetonitrile. Time-resolved fluorescence decays recorded at several wavelengths interestingly show that in the blue region of the spectrum (450 nm, see Figure S33 and Table S4, Supporting Information) the decay can be fitted with two decay time (0.70 and 3.58 ns) while at higher emission wavelengths (490, 530, and 570 nm) a third decay time around 1.2–1.3 ns appears and the short time constant around 0.6 ns becomes a rise time (negative pre-exponential coefficient see Table S4, Supporting Information). This is typical of a slow conformational change in the excited state from the emissive  $\text{E}^*$  closed-enol to the keto  $\text{K}^*$  geometry.

The theory confirmed a twisted conformation in the enol form at the ground state for 3Py-PyOHTr-10, due to the steric restriction imposed by the ethynyl 3-pyridyl substituent. Upon excitation, the molecule relaxes following a planarization path and reaching the enol closed form, before proton transfer to a keto form. The theoretical emission from  $\text{K}^*$  is 462 nm (2.68 eV) and

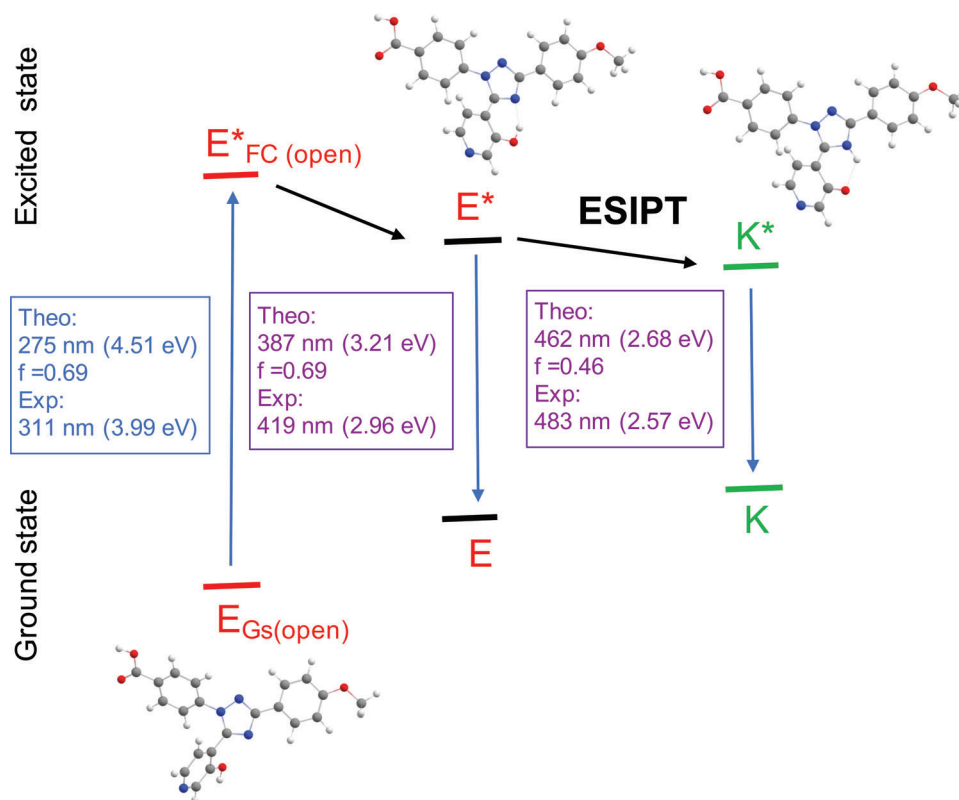


**Figure 7.** Schematic representation of absorption and emission of PyOHTr-2 in CH<sub>3</sub>CN. The excitation energies in brackets and the oscillator strengths (*f*) from time-dependent density functional theory (TD-DFT) are reported. Theoretical (Theo) and experimental values (Exp) of all observed transitions are given in nanometer (nm).

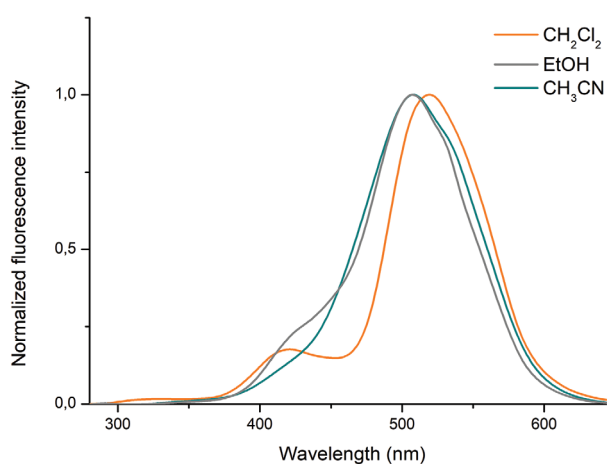


**Figure 8.** Emission spectra of 3Py-PyOHTr-10 in various solvents after excitation at 260 nm.

compared well to experiment 507 nm (2.45 eV) (Figure 8). The schematic representation of absorption of 3Py-PyOHTr-10 is in Figure S53 (Supporting Information).

We thus conclude that this spectral change arises from a cooperative ES IPT-ICT process in the 3-pyridyl ethynyl substituted triazole. As expected, the presence of expanded  $\pi$ -system modifies not only the electronic distribution but also the acidity of

the O-H donor group and thus proton transfer rate.<sup>[24]</sup> The relative population of enol/keto forms is modified at the excited state leading to the presence of a strong keto emission red-shifted in all solvents.

Finally, we have demonstrated that 3Py-PyOHTr-10 exhibits green ES IPT fluorescence (525 nm in CH<sub>2</sub>Cl<sub>2</sub>), large Stokes shift, dual emission and bright luminescence. Altogether, these appealing properties suggest the high potential of this structure to generate white light. In this area, metal complexes represent a promising category of ES IPT chromophores with enhanced optical properties, tunable emitting colors due to the structural modification of the system upon coordination.<sup>[25]</sup>

Complexation of 3Py-PyOHTr-10 with zinc salts was thus considered to explore metal coordination effect on ES IPT process and optical properties.

Notably, the presence of Zn<sup>2+</sup> change notably the absorption spectrum of 3Py-PyOHTr-10 in acetonitrile. Addition to 3Py-PyOHTr-10 of increasing amount of a 0.2 M solution of Zn(NO<sub>3</sub>)<sub>2</sub> in CH<sub>3</sub>CN leads to the formation of a new absorption bands maximizing at 292 nm and one smaller around 374 nm (Figure S35, Supporting Information).

The emission spectra are also affected by the presence of Zn<sup>2+</sup> (Figure 9). Upon excitation at 270 nm, the shortest emission fluorescence emission at 450 nm (Ee\*) of 3Py-PyOHTr-10 in CH<sub>3</sub>CN increases significantly as the concentration of Zn<sup>2+</sup> increases while the keto emission (Ke\*) is quite constant until it disappears when adding a large excess of Zn<sup>2+</sup>. Interestingly, at the

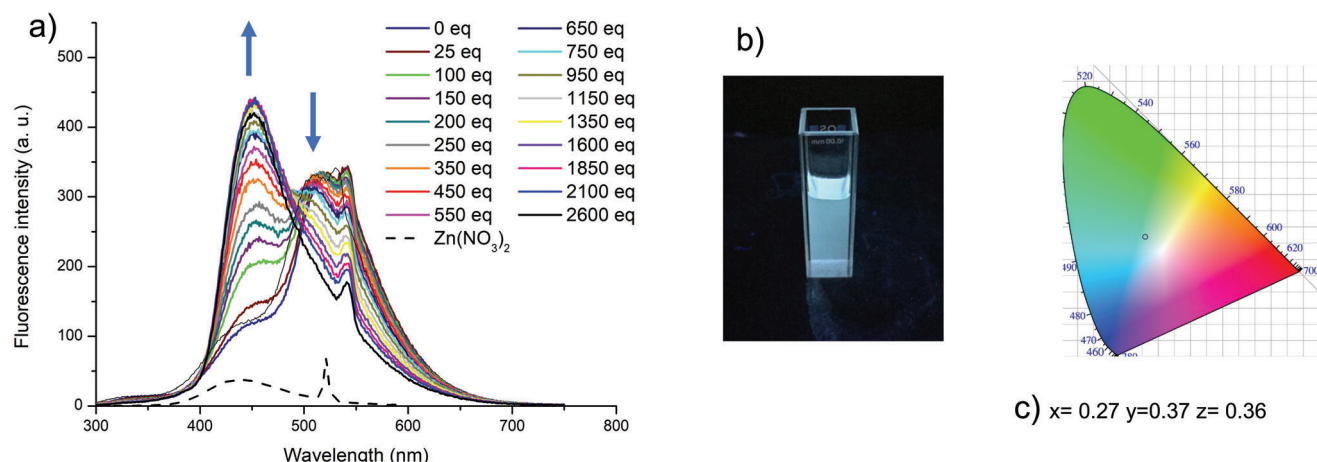


**Figure 9.** a) Emission spectra of 3Py-PyOHTr-10 (exc 270 nm) with increasing amount of  $\text{Zn}(\text{NO}_3)_2$  in DMSO/ $\text{CH}_3\text{CN}$  ( $1.6 \times 10^{-5}$  M) and  $\text{Zn}(\text{NO}_3)_2$  alone to see of diffusion. b) Photographs of 3Py-PyOHTr-10 + 812 equiv. of  $\text{Zn}(\text{NO}_3)_2$  under UV illumination at 365 nm in DMSO/DCM. c) CIE chromaticity diagram of 3Py-PyOHTr-10 + 812 equiv. of  $\text{Zn}(\text{NO}_3)_2$  in DMSO/DCM (1/99).

ratio of 812:1 in equivalent (Zn/10) in  $\text{CH}_2\text{Cl}_2$  solution, the putative complex **Zn-10** exhibits a whitish bright luminescence to the naked eye under irradiation at 365 nm with CIE coordinates  $(x,y,z) = (0.27, 0.37, 0.36)$  (Figure 9). This effect is certainly a consequence of the combination of ESIPT and normal enol emission of the complex. Rationalization of the optical behavior of **Zn-10** by complexation studies is under investigation. These studies will provide a valuable insight into ESIPT mechanism of these fluorophore and the origin of the white light luminescence.

### 3. Conclusion

In this study, we showed that pyridine substituted 1,2,4-triazole, PyOHTr are solvatochromic emitters with large Stokes shift and, for some of them in less polar solvents present a dual emission. We also demonstrated that PyOHTr's ESIPT fluorescence can be fine-tuned in both solution and solid state, by varying the electronic properties of the structure. Our theoretical investigation of the ground and excited states of a representative PyOHTr, in several solvents, using TD-DFT supported our observations.

Though most of the PyOHTr systems showed weak fluorescence in solution, some of them displayed an enhanced fluorescence in solid state or a panchromatic behavior upon coordination with  $\text{Zn}^{2+}$  cation leading to white light emission.

Therefore, PyOHTr derivatives can be considered as promising fluorescent molecules with unique optical properties for the development of a new class of efficient ESIPT fluorophores with high potential of applications in both medicinal chemistry and materials science.

### Supporting Information

Supporting Information is available from the Wiley Online Library or from the author.

### Acknowledgements

The authors thank Sorbonne Université and CNRS for funding, the Fédération de Recherche de Chimie Moléculaire de Paris Centre (FR2769) for

providing technical access to analytical instruments. The authors thank Interface pour le vivant doctoral program from Sorbonne Université for a PhD grant to A.N.-D. The authors gratefully acknowledge Arnaud Brosseau (PPSM) for his help with the TCSPC measurements.

### Conflict of Interest

The authors declare no conflict of interest.

### Data Availability Statement

The data that support the findings of this study are available in the supplementary material of this article.

### Keywords

1,2,4-triazole, ab initio calculations, excited state intramolecular proton transfer (ESIPT), fluorescence, solid-state emission, Stokes shift, white light

Received: February 10, 2023

Revised: March 12, 2023

Published online:

- [1] a) T. Xiao, C. Bao, L. Zhang, K. Diao, D. Ren, C. Wei, Z.-Y. Li, X.-Q. Sun, *J. Mater. Chem.* **2022**, *10*, 8528; b) V. Padalkar, S. Seki, *Chem. Soc. Rev.* **2016**, *45*, 169; c) J. Zhao, S. Ji, H. Gui, P. Yang, *Phys. Chem. Chem. Phys.* **2012**, *14*, 8803; d) J. Wu, W. Liu, J. Ge, H. Zhang, P. Wang, *Chem. Soc. Rev.* **2011**, *40*, 3483.
- [2] a) K. Diao, D. J. Whitaker, Z. Huang, H. Qian, D. Ren, L. Zhang, Z.-Y. Li, X.-Q. Sun, T. Xiao, L. Wang, *Chem. Commun.* **2022**, *58*, 2343; b) T. Pariat, T. Stoerkler, C. Diguët, A. D. Laurent, D. Jacquemin, G. Ulrich, J. Massue, *J. Org. Chem.* **2021**, *86*, 3763; c) C. Azarias, S. Budzák, A. D. Laurent, G. Ulrich, D. Jacquemin, *Chem. Sci.* **2016**, *7*, 3763; d) K.-I. Sakai, S. Tsuchiya, T. Kikuchi, T. Akutagawa, *J. Mater. Chem. C* **2016**, *4*, 2011.

- [3] A. C. Sedgwick, L. Wu, H.-H. Han, S. S. Bull, X.-P. He, T. D. James, J. L. Sessler, B. Z. Tang, H. Tian, J. Yoon, *Chem. Soc. Rev.* **2018**, *47*, 8842.
- [4] L. L. Falher, O. Ben Ayad, O. Ziyaret, C. Botuha, S. Thorimbert, F. Slowinski, *Eur. J. Org. Chem.* **2015**, *17*, 3830.
- [5] L. Le Falher, A. Mumtaz, A. Nina Diogo, S. Thorimbert, C. Botuha, *Eur. J. Org. Chem.* **2017**, *2017*, 827.
- [6] a) R. Kaur, A. R. Dwivedi, B. Kumar, V. Kumar, *Anti-Cancer Agents Med. Chem.* **2016**, *16*, 465; b) F. Dumur, M. Lepeltier, H. Z. Siboni, P. Xiao, B. Graff, F. Morlet-Savary, J. Lalevéé, D. Gigmes, H. Aziz, *Synth. Met.* **2014**, *195*, 312.
- [7] a) M. Shirley, G. L. Plosker, *Drugs* **2014**, *74*, 1017; b) S. Steinhäuser, U. Heinz, M. Bartholomä, T. Weyhermüller, H. Nick, K. Hegetschweiler, *Eur. J. Inorg. Chem.* **2004**, *2004*, 4177; c) U. Heinz, K. Hegetschweiler, P. Acklin, B. Faller, R. Lattmann, H. P. Schnebli, *Angew. Chem., Int. Ed.* **1999**, *38*, 2568.
- [8] P. L. Wu, X. J. Feng, H. L. Tam, M. S. Wong, K. W. Cheah, *J. Am. Chem. Soc.* **2009**, *131*, 886.
- [9] Z. H. Li, M. S. Wong, H. Fukutani, Y. Tao, *Org. Lett.* **2006**, *19*, 4271.
- [10] G. Dahm, E. Borré, C. Fu, S. Bellemin-Laponnaz, M. Mauro, *Chem. Asian J.* **2015**, *10*, 2368.
- [11] a) A. D. Beldovskaya, G. A. Dushenko, N. I. Vikrishchuk, L. D. Popov, Y. V. Revinskii, I. E. Mikhailov, *Russ. J. Gen. Chem.* **2013**, *83*, 2075; b) B. Bertrand, C. Botuha, J. Forté, H. Dossmann, M. Salmain, *Chem. - Eur. J.* **2020**, *26*, 12846; c) B. Bertrand, G. Gontard, C. Botuha, M. Salmain, *Eur. J. Inorg. Chem.* **2020**, *35*, 3370.
- [12] a) F. A. S. Chipem, A. Mishra, G. Krishnamoorthy, *Phys. Chem. Chem. Phys.* **2012**, *14*, 8775; b) S. Sahu, M. Das, A. K. Bharti, G. Krishnamoorthy, *Phys. Chem. Chem. Phys.* **2018**, *20*, 27131.
- [13] a) A. C. Sedgwick, K.-C. Yan, D. N. Mangel, Y. Shang, A. Steinbrueck, H.-H. Han, J. T. Brewster, II, X.-L. Hu, D. W. Snelson, V. M. Lynch, H. Tian, X.-P. He, J. L. Sessler, *J. Am. Chem. Soc.* **2021**, *143*, 1278; b) X.-L. Hu, A. C. Sedgwick, D. N. Mangel, Y. Shang, A. Steinbrueck, K.-C. Yan, L. Zhu, D. W. Snelson, S. Sen, C. V. Chau, G. Juarez, V. M. Lynch, X.-P. He, J. L. Sessler, *J. Am. Chem. Soc.* **2022**, *144*, 7382.
- [14] P. Dijkstra, D. Angelone, E. Talnishnikh, H. J. Wörtche, E. Otten, W. R. Browne, *Dalton Trans.* **2014**, *43*, 17740.
- [15] H. K. Fun, S. Chantrapromma, A. S. Dayananda, H. S. Yathirajan, S. Thomas, *Acta Crystallogr.* **2012**, *68*, 0792.
- [16] H. W. Yang, B. M. Craven, *Acta Crystallogr.* **2008**, *B54*, 912.
- [17] Deposition numbers 2218803 (for PyOHTr-5) and 2218804 (for PyCOTr-9) contain the supplementary crystallographic data for this paper. These data are provided free of charge by the joint Cambridge Crystallographic Data Centre, Fachinformationszentrum Karlsruhe Access Structures Service, <https://www.ccdc.cam.ac.uk/structures/>
- [18] D. Goswami, H. A. Vitorino, R. Y. P. Alta, D. M. Silvestre, C. S. Nomura, M. T. Machini, B. P. Espósito, *BioMetals* **2015**, *28*, 869.
- [19] P. Charisiadis, V. G. Kontogianni, C. G. Tsiafoulis, A. G. Tzacos, M. Siskos, I. P. Gerathanassis, *Molecules* **2014**, *19*, 13643.
- [20] V. Vogeli, W. von Philipsborn, *Org. Magn. Reson.* **1973**, 551.
- [21] L. Xu, G.-C. Guo, B. Liu, M.-L. Fu, J.-S. Huang, *Acta Crystallogr.* **2004**, *E60*, o1060.
- [22] H. Melhuish, *J. Phys. Chem.* **1961**, *65*, 229.
- [23] S. J. Kim, S. Y. Park, *J. Am. Chem. Soc.* **2004**, *126*, 11154.
- [24] K. Skonieczny, J. Yoo, J. M. Larsen, E. M. Espinoza, M. Barbasiewicz, V. I. Vullev, C.-H. Lee, D. T. Gryko, *Chem. - Eur. J.* **2016**, *22*, 7485.
- [25] K.-I. Sakai, S. Takahashi, A. Kobayashi, T. Akutagawa, T. Nakamura, M. Dsen, M. Kato, U. Nagashima, *Dalton Trans.* **2010**, *39*, 1989.